

Citation for published version:

Chu, L, Jiang, G, Hu, X, James, TD, He, X-P, Li, Y & Tang, T 2018, 'Biodegradable macroporous scaffold with nano-crystal surface microstructure for highly effective osteogenesis and vascularization', *Journal of Materials Chemistry B*, vol. 6, no. 11, pp. 1658-1667. <https://doi.org/10.1039/C7TB03353B>

DOI:

[10.1039/C7TB03353B](https://doi.org/10.1039/C7TB03353B)

Publication date:

2018

Document Version

Peer reviewed version

[Link to publication](#)

Copyright © 2018 The Royal Society of Chemistry. The final publication is available at Journal of Materials Chemistry B via <https://doi.org/10.1039/c7tb03353b>

University of Bath

Alternative formats

If you require this document in an alternative format, please contact:
openaccess@bath.ac.uk

General rights

Copyright and moral rights for the publications made accessible in the public portal are retained by the authors and/or other copyright owners and it is a condition of accessing publications that users recognise and abide by the legal requirements associated with these rights.

Take down policy

If you believe that this document breaches copyright please contact us providing details, and we will remove access to the work immediately and investigate your claim.

Biodegradable macroporous scaffold with nano-crystal surface microstructure for highly effective osteogenesis and vascularization

Received 00th January 20xx,
Accepted 00th January 20xx

DOI: 10.1039/x0xx00000x

www.rsc.org/

Linyang Chu,^a Guoqiang Jiang^b, Xi-Le Hu,^c Tony D. James,^d Xiao-Peng He,^{c*} Yaping Li^{b*} and Tingting Tang^{a*}

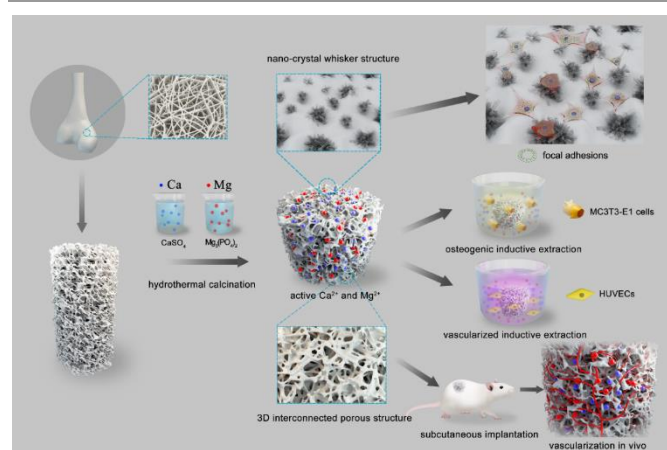
Using the hydrothermal calcination method, bovine cancellous bone was transformed into a degradable macroporous scaffold with a nano-crystal surface microstructure, capable of releasing bioactive ions. Compared with the control group, the presence of the nano-crystal microstructure of the material scaffold significantly promoted the gene expression of adhesion proteins including integrin and vinculin, thus facilitating attachment, spreading, proliferation and focal adhesions formation of MC3T3-E1 cells on the surface of the scaffold. Additionally, the release of active magnesium and calcium ions from the scaffold promoted expression of osteogenic genes and formation of calcium nodules in osteoblasts. Both *in vitro* and *in vivo* assays demonstrated that the three-dimensional interconnected porous architecture promoted vascularization and tissue integration. Our findings provide new insight into the development of degradable macroporous composite materials with “three-dimensional” surface microstructures as bone substitutes or tissue engineering scaffolds with potential for clinical applications.

1. Introduction

In the design and development of bone substitute or tissue engineering scaffold, it is important to take into account the complex composition and microstructure of mineralized human tissues.¹⁻³ An ideal material for bone repairing or regeneration should be biocompatible, biodegradable, and bioactive for osteogenesis and vascularization. This requires the construction of well interconnected three-dimensional structures and bioactive surfaces to facilitate the migration, adhesion and proliferation of bone cells.⁴⁻⁷ In addition, bone substitutes or scaffolds should be degradable over time to provide space for bone and blood vessel growth.⁸⁻¹¹

Hydroxyapatite (HA, $\text{Ca}_5(\text{PO}_4)_3(\text{OH})$) and β -TCP ($\text{Ca}_3(\text{PO}_4)_2$) are widely used bone repairing materials in clinical medicine because of their recognized compatibility and osteoconductivity. However, HA is very stable in the body, which compromises the balance between bone growth and material degradation.¹² β -TCP is much more degradable than HA *in vivo*, but the unpredictable degradation rate and low

mechanical stability limit its real application in bone regeneration.^{13, 14} To overcome these problems, multiphase bio-composite materials produced by a variety of techniques have been developed as bone substitute with well-balanced surface structure, pore size and connectivity, as well as degradation rate.^{15, 16}



Scheme 1. Schematic illustration of the degradable macroporous scaffold with nano-crystal surface microstructure and capable of releasing bioactive ions. Both *in vitro* and *in vivo* assays were used to evaluate the cytocompatibility, osteogenesis, vascularization and tissue integration of the scaffold.

Herein, we have used the hydrothermal calcination method to achieve the conversion of bovine cancellous bone (HA as main ingredient) into degradable macroporous scaffold (HA/Ca/Mg). After hydrothermal reaction with additions of Mg^{2+} , PO_4^{3-} and SO_4^{2-} , the composite material retained its

^a Shanghai Key Laboratory of Orthopedic Implants, Department of Orthopedic Surgery, Shanghai Ninth People's Hospital, Shanghai Jiao Tong University School of Medicine, Shanghai 200011, P.R. China, E-mail: ttt@sjtu.edu.cn (T.-T. Tang)

^b Department of Orthopaedic Surgery, Affiliated Hospital of School of Medicine, Ningbo University, Ningbo 315211, P.R. China, E-mail: liyaping36@126.com (Y.-P. Li)

^c Key Laboratory for Advanced Materials & Feringa Nobel Prize Scientist Joint Research Center, East China University of Science and Technology, Shanghai 200237, P.R. China, E-mail: xphe@ecust.edu.cn (X.-P. He)

^d Department of Chemistry, University of Bath, Bath, BA2 7AY, U.K.

original three-dimensional interconnected porous structure. Most importantly, nano-crystal, whisker microstructure was formed on the surface, which significantly improved the cell attachment and proliferation. Furthermore, the multiphase composite is degradable, capable of releasing bioactive Mg^{2+} and Ca^{2+} ions in microenvironment. The Mg^{2+} and Ca^{2+} ions are essential elements in human body and participate in many important metabolic activities.¹⁷ It has been shown that Mg^{2+} and Ca^{2+} ions can effectively promote osteogenesis during bone repairing.^{18, 19} Since a bone substitute or scaffold should also be in favor of vascularization accelerating formation of new bones, here the vascularization of the material developed was also investigated systematically *in vitro* and *in vivo*. We believe that our composite material developed with a special, “three-dimensional” surface microstructure and the ability to release bioactive components will be a promising class of bone substitute and tissue engineering scaffold.

2. Experimental Section

2.1 Materials

Bovine bone from femoral condylar cancellous bone were cut into raw bones, which then were placed in autoclave for heating about 40-60min at 115°C. Then the resulting material was cleaned with ultrasound 4-5 times. The treated raw bones were calcined at 800°C for 6h. After cooling, a macroporous scaffold was obtained. A compound solution including Mg^{2+} , PO_4^{3-} and SO_4^{2-} was prepared with ion concentrations of 0.075mol/L, 0.1mol/L and 0.4mol/L, respectively. The calcined bone and compound solution were mixed with a mass/volume rate of 100mg/mL for hydrothermal reaction of 36h at 75°C. Then the scaffold was taken out and dried at 100°C for 24h. Finally, the scaffold was placed in temperature-controlled calcination furnace at 1050°C (temperature rise rate was 2.5°C/min) for 6h to produce the desired macroporous HA/Ca/Mg composite. HA calcined bone without hydrothermal reaction and that hydrothermally reacted in Mg^{2+} and PO_4^{3-} solution (HA/Mg) were produced by the same protocol as controls. All specimens were sterilized by ethylene oxide for 3h before cellular and animal test.

2.2 Composition and surface characteristics

The composition of scaffolds was analyzed using X-ray diffraction (XRD, Japan). The scaffolds were dried through an ethanol series, coated by gold sputtering, and examined using a scanning electron microscope (SEM, Japan) at an electron acceleration voltage of 1.5kV in secondary electron detection mode. The element distribution of scaffolds was determined using energy dispersive spectroscopy (EDS, Japan) at an electron acceleration voltage of 1.5 kV.

2.3 Microstructure measurement

The three-dimensional structure, porosity, pore connectivity and average pore size of the scaffolds were evaluated using a high-resolution micro-CT (μCT , Switzerland) at an isometric resolution of 25 μm ; data were analyzed by procedures of micro-CT (RATOC, TRI/3D-bone).

2.4 Degradation test *in vitro*

The degradation of test was carried out by previously reported study methods.²⁰ Briefly, the scaffolds were immersed into 50mM Tris-HCl solution at pH 7.40, 37°C maintaining a weight-to-volume ratio of 0.2g/mL with a shaking speed at 100 r/min. At different time point, the scaffolds were removed and cleaned with deionized water, dried at 90°C for 24h. The scaffolds were re-immersed into fresh Tris-HCl solution with the same condition. This process was repeated over a period of 4 weeks. The percentage of degradation was calculated by the following equation:

$$\text{Degradation (\%)} = 100 \times (W_0 - W_t)/W_0$$

where W_0 is the initial weight of materials and W_t is the weight after treatment over time (t).

At each time point (6, 12, 24, 72 and 168h), the scaffolds were taken out, and the concentration of Mg^{2+} , Ca^{2+} and PO_4^{3-} in Tris-HCl solution were estimated using an inductively coupled plasma optical emission spectrometer (ICP-OES, USA). Meanwhile, the scaffolds were immersed into Dulbecco's Modified Eagle's Medium at same weight-to-volume ratio and dissolution conditions mentioned above. At each time point, the pH values were measured using a flat membrane microelectrode (PB-10, Germany). All experiments were run in triplet.

2.5 Evaluation of cytocompatibility *in vitro*

2.5.1 Cell spreading and focal adhesions formation

HA, HA/Mg, and HA/Ca/Mg scaffolds (column, 10×2mm) were placed in 24-well plates. We chose the MC3T3-E1 cells,²¹ a mouse preosteoblast line derived from mouse calvaria, since they have better stability in differentiation and cell phenotype, and less individual variation than human derived stem cells; these merits may lead to better reproducibility in experimentation. The cell suspension was seeded at a density of $3.0 \times 10^4/\text{cm}^2$ for each well. To assess cell spreading and focal adhesions formation after 6 h culturing, SEM and fluorescence staining were used. Briefly, cells were cultured on scaffolds for 6h, fixed with 2.5% glutaraldehyde for 15min, and then washed three times with PBS. Next, the samples for SEM analysis were treated in the same way as the above. Meanwhile, for fluorescence staining, cells on scaffolds were fixed with 4% paraformaldehyde for 15min, permeabilized with 0.1% Triton X-100 in PBS for 10min and blocked with 5% albumin from bovine serum albumin (BSA). Then rabbit monoclonal antibody to vinculin (ab196454, Abcam) were used to stain the focal adhesions. Simultaneously, 4,6-diamidino-2-phenylindole (DAPI, Sigma) was used to stain the cell nuclei and rhodamine phalloidin (Molecular Probe, Cytoskeleton) was used to stain the filamentous actin of the cytoskeleton. At last the samples were observed by confocal laser scanning microscopy (CLSM, Germany).

To study the focal adhesions formation, intracellular integrin $\beta 1$ and vinculin protein levels at 6h were semi-quantitatively analyzed by western blotting. Collected proteins were separated using 8% SDS-PAGE gel, transferred onto PVDF membrane, and blocked with 5% skim milk solution for 1h at

room temperature. The samples were incubated with primary antibodies overnight and then incubated with an HRP-conjugated secondary antibody. Luminescence was detected and quantified by an imaging system (ChemiScope3600MINI, China). GAPDH was used as a loading control.

2.5.2 Cell attachment, viability and proliferation

As described above, the cells were co-cultured with the material in 24-well plates. The cell counting kit-8 (CCK-8) assay was used to analyze cell attachment at 6 and 12h, and to analyze cell viability and proliferation at the time points of 1, 4 and 7d. The modified OD values at 4 and 7d were normalized to those at 1d to calculate the proliferation rate of cells. In addition, fluorescence staining was used to observe cell viability on scaffolds at 1d. DAPI and rhodamine phalloidin were used to stain the cell nuclei and cytoskeleton. Cells were imaged by CLSM.

2.6 Osteogenic differentiation *in vitro*

2.6.1 Cell culture and preparation of osteogenic inductive extraction

Extraction medium of HA, HA/Mg, and HA/Ca/Mg scaffolds were prepared according to the International Organization for Standardization method (ISO 10993-12).²² Briefly, the scaffolds were incubated in standard culture medium at a mass/volume ratio of 100mg/mL at 37°C. After 24h, the supernatant was carefully collected and added with osteogenic inductive supplements, including 100nM dexamethasone (Sigma), 50µg/mL ascorbic acid (Sigma) and 10mM β-glycerophosphate sodium (Sigma). Then the osteogenic inductive extraction was filter sterilized and stored at 4°C for further use. Afterwards, MC3T3-E1 cells were cultured with standard culture medium at a density of $5.0 \times 10^4/\text{cm}^2$ in 24-well plates for 24h. Then the medium was changed to the osteogenic inductive extraction and refreshed every two days.

2.6.2 ALP, alizarin red staining and relative quantitative analysis

After 7, 14 and 21d of culture, ALP staining method was performed according to previously reported procedure.²³ ALP activity was determined using a ALP microplate test kit (Beyotime, China) and observed directly by optical microscopy. The quantity of ALP in the cell lysates was measured at 520nm using the Synergy HT microplate reader (Bio-Tek), then it was normalized to the corresponding total protein content determined by a BCA protein assay kit (ThermoFisher Scientific) according to the provided protocol. Meanwhile, calcium deposition (mineralization) was assessed by Alizarin Red S staining.²³ After culture for 21 and 28d, cells were fixed in 4% paraformaldehyde for 15min at 37°C prior to being stained with 1% alizarin red solution (Sigma) for 45min. Then the samples were washed with PBS to remove the non-specific staining and observed directly by optical microscopy. For the quantitative analysis, 10% cetylpyridinium chloride (Sigma) in 10mM sodium phosphate (Sigma) was added to the stained wells and then the

mixed solutions were measured at 620nm using the Synergy HT microplate reader (Bio-Tek).

2.6.3 Expression of osteogenic related genes

The mRNA expression of several osteogenic differentiation-related genes, including osteocalcin (OCN), bone sialoprotein (BSP), collagen type I (COL1) and osteopontin (OPN), were quantitatively determined by real-time polymerase chain reaction (PCR).²¹ The transcription levels of the genes were normalized to the housekeeping gene GAPDH. The sequences of the forward and reverse primers were demonstrated in **Table 1**. After 7, 14 and 21 days of culturing with the osteogenic inductive extraction, the TRIzol reagent (Ambion, USA) was used to collect total RNA according to the provided manufacturer's instructions. Then, reverse transcription was performed following the protocol of the Revert Aid first-strand cDNA synthesis kit (Fermentas, USA). Quantitative PCR (qPCR) was performed on an ABI 7500 machine (Applied Biosystems, USA) using the SYBR premix EX Taq PCR kit (Takara).

Table 1 Primer sequences for real-time PCR.

Target gene	Primers (5' -3' ; F = forward; R = reverse)	Length
ALP	F: GGGCATTGTGACTACCACTCG	21
	R: CCTCTGGTGGCATCTCGTTAT	21
COL 1	F: AACAGTCGCTTCACCTACAGC	21
	R: GGTCTTGGTGGTTTTGTATTCCG	22
OPN	F: CTTTCACTCCAATCGTCCCTAC	22
	R: CCTTAGACTACCGCTCTTCAT	22
OCN	F: GGACCATCTTTCTGCTCACTCTG	23
	R: TTCCTACCTATTGCCCTCCTG	23
GAPDH	F: AGGTCGGTGTGAACGGATTTG	21
	R: GGGGTCGTTGATGGCAACA	19

2.7 Bioactivity of vascularization *in vitro*

2.7.1 Cell culture and preparation of vascularized inductive extraction

Human umbilical vein endothelial cells (HUVECs) were purchased from Shanghai Institutes for Biological Science and cultured in α-minimum medium supplemented with 10% fetal bovine serum and 1% penicillin/streptomycin. The extracts medium of scaffolds, as mentioned above, was added with 1% ECGS (Endothelial Cell Growth Supplement, BD Biosciences). After that, the vascularized inductive extraction was filter sterilized and stored at 4 °C for use.

2.7.2 Capillary connections formation assay and quantitative analysis of VEGF

HUVECs were cultured in vascularized inductive extraction for 2d. Then, Matrigel (BD Biosciences) was mixed with culture media at a ratio of 1:3 and added evenly to each well of a 96-well plate. HUVECs were separately resuspended and seeded on the gel at a density of 2×10^4 cells/well. After incubation for 4h at

37°C, the plate was observed by optical microscopy. At least 5 fields were digitally acquired for each substrate and the total number of capillary connections per field were counted by a blinded observer using Image-Pro Plus software (Media Cybernetics, USA). Moreover, HUVECs were cultured in the vascularization inductive extraction for 12, 24 and 48h. At each time point, the supernatant was collected and stored at -80 °C. The concentration of VEGF was determined by using a Human Quantikine ELISA kit (R&D Systems, Canada) according to the manufacturer's instructions. Briefly, the supernatant was added to 96-well microplates that were coated with a monoclonal antibody to the factor of interest and incubated for 2h. After washed with PBS, substrate solution was added and incubated for 30min, and the reaction was terminated by addition of stop solution. VEGF levels were determined by measurement of the optical density at 450nm using the Synergy HT microplate reader (Bio-Tek).

2.8 Tissue integration and vascularization analysis *in vivo*

2.8.1 Subcutaneous implantation of scaffolds in mice

A dorsum subcutaneous implantation model was established to evaluate vascularization of scaffolds *in vivo*.²⁴ All experimental procedures were approved and performed in accordance with the guidelines of the Animal Ethics Committee of Shanghai Ninth People's Hospital (The protocol registry number: A-2016-017). Briefly, 24 specific pathogen-free (SPF) 8-week-old male BALA/c mice were assigned randomly to three groups. The mice were initially anesthetized by using an intraperitoneal injection of 1% pentobarbital sodium (100mg/kg) and the left dorsum was shaved and cleaned with 2% iodine prior to the procedure. Then, a deep subcutaneous pocket was made through an approximately 1.5cm longitudinal skin incision over the left dorsum, in which one sample of a sterile scaffold was placed. The mice were housed in ventilated rooms and allowed to eat and drink after surgery. No antibiotics were administered, and no mortality occurred during experiment.

2.8.2 Micro-CT based vascularization and histological analysis

Microfil perfusion (Microfil MV, USA) was conducted at 28 days after surgery. Briefly, after the pericardial cavity of the mice was exposed, the right auricle was snipped, then immediately heparinized saline (100U/mL) was perfused into the apex of the heart at 2mL/min using a syringe pump. A solution of Microfil prepared in a volume ratio of 4/5 of Microfil/diluent with 5% curing agent was perfused at a rate of 2mL/min according to the manufacture's protocol.²⁴ Then implanted scaffolds were harvested, fixed with 4% neutral-buffered formaldehyde for 48h and decalcified with 9% formic acid for 4 weeks. The vascularization of scaffolds was reconstructed using micro-CT. Three-dimensional reconstruction of the newly formed vessels and their volume within scaffolds were analyzed by the software provided by manufacture. The evaluation was obtained from four animals randomly selected in each group.

After that, remaining scaffolds and surrounding soft tissues were retrieved 28 days after surgery. Then they were immersed in 4% neutral-buffered formaldehyde for 48h. The collected scaffolds and surrounding soft tissues were embedded into

paraffin. The specimens were cut into sections parallel to the top surface of the scaffolds and prepared at a thickness of 5µm (EXAKT-400, German). Hematoxylin eosin (H&E) and Masson's trichrome staining were used to assess the morphology and tissue integration. Furthermore, CD31 immunohistochemistry was used to assess vascularization. Sections were dewaxed in descending concentrations of alcohol and rehydrated. The slides were immersed in 3% hydrogen peroxide to block endogenous peroxidases and rinsed in PBS. They were immersed in 0.1% Triton-X100 in PBS for 15min to allow penetration of the membrane. Antigen retrieval was carried out in a 10mM warm citrate buffer for 15min. Specific sites were saturated with normal goat serum, for 40min at 37 °C. Then, monoclonal anti-CD31 antibody (ab76533, Abcam) was used. The sections were incubated with biotinylated rabbit anti-rabbit immunoglobulins, washed in TBS for 5min and incubated for 30min with streptavidin-peroxidase (1:50, DAKO). The nuclei were counter stained with H&E for two to three seconds, washed in distilled water and finally covered with Aqua Tex (Merck, Germany). Four slides were then examined microscopically for taking its average for statistical analysis.

2.9 Statistical analysis

All data are expressed as Mean ± SD. Nonparametric test (Mann–Whitney U test), one-way analysis of variance (ANOVA) and the least significant difference (LSD) test were utilized to determine the level of significance; $p < 0.05$ was defined as statistically significant, and $p < 0.01$ was considered highly statistically significant. All statistical analyses of the data were performed using SPSS software (v19.0, USA).

3. Results and discussion

3.1 Composition and microstructure characteristics

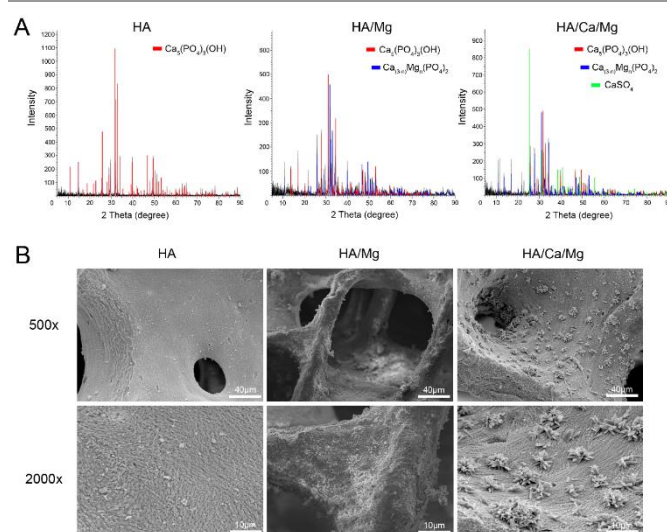


Fig 1. Composition and surface characteristics of different scaffolds. (A) X-ray diffraction of scaffolds. (B) SEM images of the surface morphology of scaffolds.

In this study, the hydrothermal calcination method has been used to convert bovine cancellous bone into multiphase,

degradable macroporous scaffold. The hydrothermal calcination process is necessary since it can remove immunogenic proteins and collagen, maintain the original three-dimensional interconnected porous structure and facilitate the formation of surface microstructure. The composition and microstructures of the different scaffolds constructed were first characterized by a diverse range of techniques. **Fig.1A** showed the main composition of different scaffolds by XRD. The results showed that HA scaffold was mainly composed of hydroxyapatite, in contrast, after calcination with hydrothermal reaction, $\text{Ca}_{(3-n)}\text{Mg}_n(\text{PO}_4)_2$ was produced in HA/Mg scaffold. Moreover, in HA/Ca/Mg scaffold, we observed that the content of $\text{Ca}_{(3-n)}\text{Mg}_n(\text{PO}_4)_2$ was relatively decreased along with the emergence CaSO_4 signal. The surface morphology of three scaffolds constructed was characterized using SEM (**Fig.1B**). The images showed that the HA/Mg scaffold had a rougher surface than HA scaffold, which could be ascribed to the formation of $\text{Ca}_{(3-n)}\text{Mg}_n(\text{PO}_4)_2$ on the former surface. The elemental distributions of Ca, O, P, Mg, and S of different scaffolds obtained by EDS are shown in **Fig.2A**. The images showed that Mg and S elements existed in HA/Ca/Mg scaffold after hydrothermal reaction. A weaker Mg element signal was observed in the HA/Ca/Mg scaffold than the HA/Mg scaffold, which was consistent with the results of XRD analysis. Interestingly, after calcination we observed the formation of a nano-crystal, whisker-like microstructure on the surface of the HA/Ca/Mg scaffold (**Fig.1B**). Meanwhile, EDS analysis of nano-crystal whisker on HA/Ca/Mg scaffold surface suggests that the composition consisted of sulfur element (**Fig.2A**). The results of XRD and EDS analyses demonstrated that the main composition of the nano-crystal whisker structure was CaSO_4 .

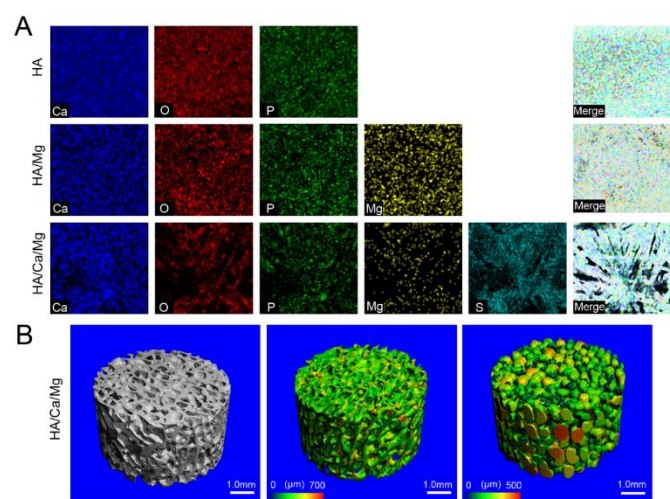


Fig. 2. Element distribution of scaffolds and 3D microstructure of HA/Ca/Mg scaffold. (A) Element distribution on surface of various scaffolds. (B) 3D reconstructed images, porosity, pore connectivity and pore size of HA/Ca/Mg scaffolds obtained using Micro-CT.

A bioactive scaffold should exhibit an ideal porosity with a homogeneous and interconnected porous structure, which is amenable for bone repair, vascular access and oxygen and tissue fluid exchange, providing physiologically active space for bone ingrowth.^{25, 26} The morphology and pore distribution of

HA/Ca/Mg scaffold were characterized using micro-CT (**Fig.2B**). The scaffold possessed homogeneous and interconnected porous structures with a porosity of $82.4 \pm 4.1\%$, connectivity of 100% and an average pore size of $370.3 \pm 37.6\mu\text{m}$. There is no significant difference in the porous structures among all three groups.

3.2 Degradation test *in vitro*

Degradation rate is another important feature of bone substitutes and bone-tissue engineering scaffolds.²⁷ The ability of a scaffold to degrade within a reasonable timeframe can offer space for new bone formation and blood vessel growth. Whereas the degradation rate of HA is thought to be too slow for new bone growth, too fast degradation rate would lead to unwanted bone defects in the implanted area.^{12, 13, 28, 29} The degradation of different scaffolds was measured in Tris-HCl solution. As shown in **Fig.3A**, the weight loss of HA/Ca/Mg scaffold after 4 weeks was about 21.8%, which is larger than that of the HA/Mg and HA group. The pH value of HA/Mg scaffold increased rapidly within 0-24h, and from 24 to 168h, the pH continued to increase slightly. The HA/Ca/Mg scaffold had a relatively smaller pH fluctuation during 0 to 168h. Due to limited degradation, the pH value of HA scaffold hardly changed with time. Shown in **Fig.3C-E** are the concentration changes of Mg^{2+} , Ca^{2+} and PO_4^{3-} released from different scaffolds. The concentration of Mg^{2+} , Ca^{2+} and PO_4^{3-} in HA/Mg and HA/Ca/Mg increased rapidly from 0 to 72h and began to stabilize from 72 to 168h. In contrast, no significant changes in ion concentration of the HA scaffold were observed at different time points. Mg^{2+} plays a critical role in the body in mediating cell-extracellular matrix (ECM) interactions and controlling bone apatite structure and density.^{30,31} The HA/Ca/Mg scaffold contains three different main ingredients and the dissolution rate between the various composition was largely difference. Therefore, the scaffold could achieve gradient degradation, i.e. the material could be degraded rapidly in early stage to release active Mg^{2+} , Ca^{2+} and PO_4^{3-} , followed by a stably sustained degradation to offer space for new bone formation.

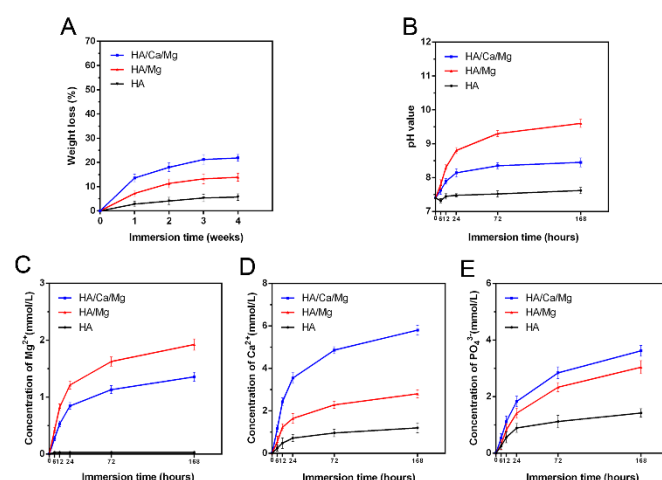


Fig. 3. Degradation test. (A) Weight loss rate of different scaffolds. (B) Changes in pH value. (C), (D), (E) Changes in concentration of Mg^{2+} , Ca^{2+} and PO_4^{3-} .

3.3 Cell attachment, spreading, proliferation and focal adhesions formation on the scaffold surface

SEM was used to observe cell morphology on different scaffolds after 6h. **Fig.4A** showed less adherent cells on HA and HA/Mg

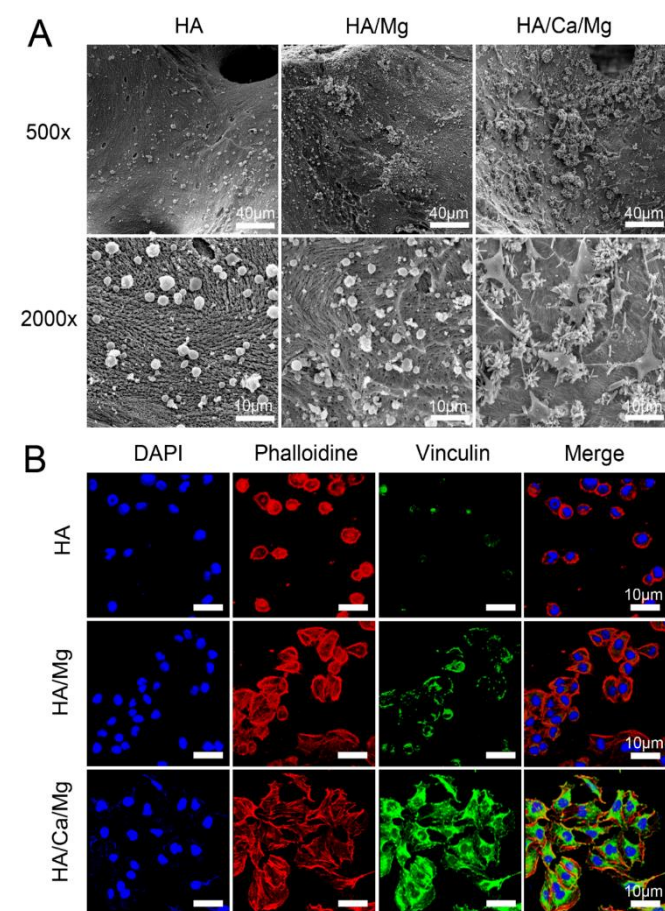


Fig. 4. Spreading and focal adhesions formation of MC3T3-E1 cells on the different scaffolds. (A) SEM images of cells morphology and spreading at 6h on scaffolds. (B) The cytoskeletal morphology and focal adhesions formation of cells at 6h on scaffolds. Representative images of cells stained with DAPI for cell nuclei (blue), rhodamine phalloidine for actin filaments (red), and monoclonal antibody for focal adhesions (green). For CLSM, the scale bar for the row is shown in the merge image.

scaffolds than on the HA/Ca/Mg scaffold. In particular, on the HA/Ca/Mg scaffold, cells were densely adhered to the nano-crystal whisker microstructure on which numerous filopodia were pervaded. From mechanism of view, excellent cell spreading might be caused by an increased expression of adhesion related proteins including integrins and vinculin, thereby providing mechanical forces to the material surface.³² Integrins are a family of transmembrane receptors that provide anchorage force for cellular adhesion by activating intracellular signalling pathways after ligand binding.³³ It is proven that the expression of integrins is dependent on structure, roughness and wet ability of material surface.³² Vinculin, on the other hand, a highly conserved actin-binding protein, is frequently used as a marker for focal adhesion.³⁴ Shown in **Fig.4B** is the CLSM micrograph exhibiting cell spreading and focal adhesions formation on the different scaffolds. The cells grown on HA/Ca/Mg scaffold displayed a clustered and confluent

morphology with extensive actin filaments linking to adjacent cells. In contrast, cells on HA and HA/Mg scaffolds exhibited dispersed morphology with fewer actin filaments and a more reduced level of spreading. Meanwhile, the vinculin protein was immune-stained in the cytoplasm (visible as a green background inside the cells), suggesting the formation of abundant focal adhesions on HA/Ca/Mg. The intracellular protein expression of integrin $\beta 1$ and vinculin after 6h was further analyzed by western blotting (**Fig.5A-B**). The results showed that integrin $\beta 1$ and vinculin were detected at higher levels in cells grown on HA/Ca/Mg scaffold ($p < 0.01$) than other scaffolds, which suggested that the microstructure of HA/Ca/Mg scaffold could up-regulate expression of focal adhesions proteins in MC3T3-E1 cells, in agreement with the results of CLSM.

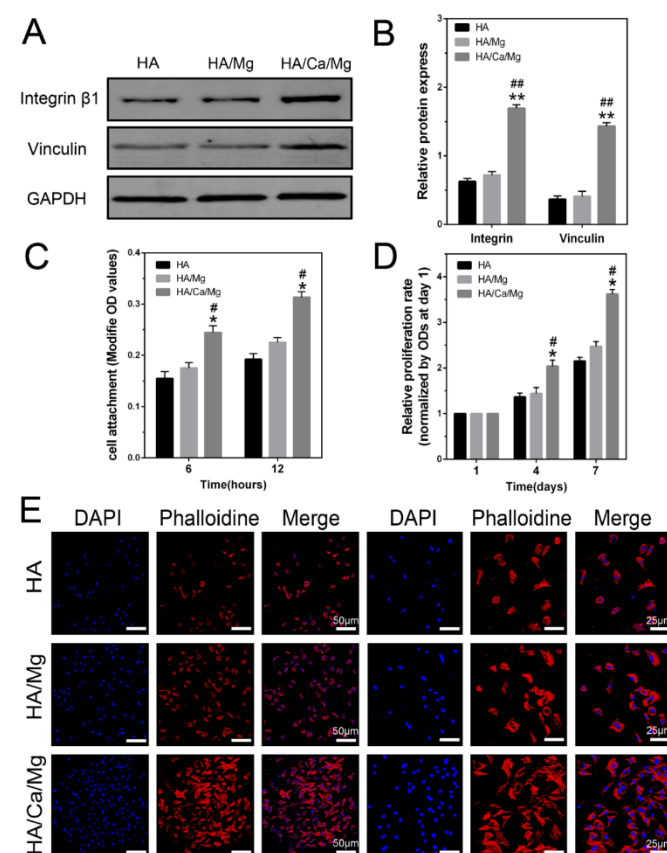


Fig 5. Adhesion related protein expression, attachment, viability and proliferation of MC3T3-E1 cells on the different scaffolds. (A), (B) Western blotting for analysis of integrin $\beta 1$ and vinculin in cells cultured for 6h and the results were quantified. (C) Cell attachment analysis at 6 and 12h determined by CCK-8 assay. (D) Relative cell proliferation rates at 4 and 7d determined by CCK-8 assay. (E) Cell viability evaluated by fluorescence staining at 1d on scaffolds. DAPI for cell nuclei (blue) and phalloidine for actin filaments (red). * $p < 0.05$ compared with HA scaffolds. ** $p < 0.01$ compared with HA scaffolds. *** $p < 0.01$ compared with HA/Mg scaffolds. The scale bar for the row is shown in the merge image.

Cell attachment on scaffolds was evaluated by CCK-8 assay after 6 and 12h. As shown in **Fig. 5C**, the counts of adherent cells on HA/Ca/Mg scaffold were significantly higher than that on HA and HA/Mg scaffolds at 6 and 12h ($p < 0.05$). This result suggests that HA/Ca/Mg scaffold could improve cell initial attachment on

the material surface. We deduced that the initial cell attachment and spreading would affect cell proliferation on the material surface. This deduction was proven by the following analysis. The relative proliferation rate of cells on different scaffolds was shown in Fig.5D. The cells on HA/Ca/Mg scaffold exhibited a higher proliferation rate than those on HA and HA/Mg scaffolds at 4 and 7d ($p < 0.05$). In addition, although the proliferation of cells on HA/Mg scaffold was slightly higher than that on HA scaffold, no significant differences were observed between the two scaffolds from day 1 to 7d ($p > 0.05$). Moreover, CLSM was used to observe cell viability at 1d. The cells stained with DAPI and phalloidine on the three scaffolds at 1d were showed in Fig.5E, which again corroborated the higher cell viability on the HA/Ca/Mg scaffold than other scaffolds. These results confirmed that the nano-crystal microstructure could promote cell attachment, spreading, proliferation and focal adhesions formation, thus improving cytocompatibility of the scaffold. In our previous study,³⁵ we demonstrated that the topographical and morphological features of the nanostructured surface could regulate cell extension and cytoskeleton tension by the related signalling pathway of focal adhesions, which is similar to the results when using a HA/Ca/Mg scaffold. With this study we envisioned that these biological effects might be related to the unique characteristics of the nano-crystal whisker-like structure, the nano-topological effect, and the enhanced adhesion protein adsorption level. Additional, relevant research will be carried out in the near future to confirm these theories. Moreover, we have already proven that the material's nano-surface could regulate osteogenic differentiation by affecting cell adhesion.³⁶ The cell adhesion mediated the activity of intracellular YAP/TAZ signalling by mechanotransduction, which could activate osteogenesis-related pathways and further promote the differentiation of cells. The focal adhesions formation plays a critical role in transformation of physical characteristics into biological effects.

3.4 Osteogenic differentiation *in vitro*

The role of bioactive Ca^{2+} and Mg^{2+} are beneficial for proliferation and differentiation of osteoblasts in osteogenesis process.^{8, 17, 37, 38} Moreover, extracellular PO_4^{3-} can enter cells and subsequently the mitochondria, thereby promoting the synthesis of ATP. The ATP is then secreted, which can accelerate osteogenic differentiation of osteoblasts in bone regeneration by autocrine and/or paracrine signalling pathways.³⁹ The ALP, Alizarin-red staining and relative quantitative analysis were carried out to better understand the influence of bioactive extraction of the scaffolds on the osteogenic differentiation of cells. Fig.6A-B showed the ALP and Alizarin-red intensity after 7, 14, 21 and 28d of cell culturing. The intensity of HA/Ca/Mg group was considerably stronger than HA and HA/Mg groups. The relative ALP activity of HA/Ca/Mg group was evidently higher than that of the HA group at all time points (Fig.6C, $p < 0.01$). The results also indicated that the calcium nodule formation of HA/Ca/Mg group was significantly higher than that on HA and HA/Mg groups at 21 and 28d (Fig.6D, $p < 0.01$). Meanwhile, we examined the expression lever of several critical

osteogenic markers using quantitative real-time PCR assay at 7, 14 and 21d (Fig.7A-D). At 7d, cells grown in osteogenic inductive extraction of HA/Ca/Mg scaffold showed higher expression levels of ALP and COL1 compared with other groups ($p < 0.05$). At 14d, the gene expression of COL1 and OPN reached the peak in all three groups, and the ALP, COL1, OPN, and OCN mRNA levels of HA/Ca/Mg group were significantly higher than that of the HA and HA/Mg groups ($p < 0.05$). Besides, at 21d, the expression of four osteogenic mRNA of HA/Ca/Mg group still maintained the highest level in all groups ($p < 0.05$). These results showed that osteogenic inductive extraction of HA/Ca/Mg scaffold could lead to a better osteogenesis ability than the other control scaffolds.

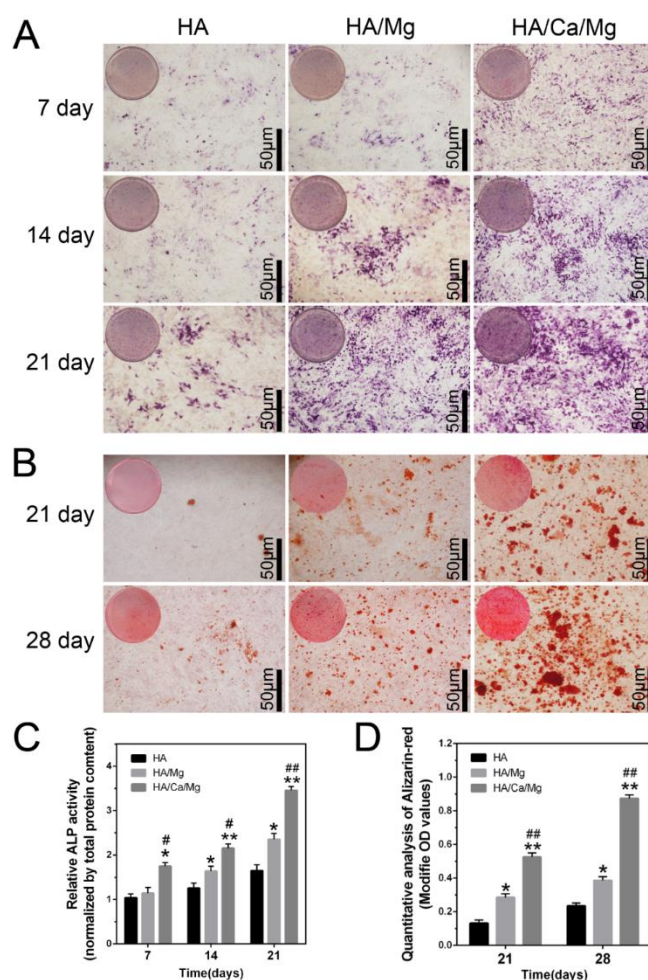


Fig 6. Effects of osteogenic inductive extraction of scaffolds on osteogenesis of MC3T3-E1 cells. (A) ALP staining after 7, 14 and 21d of cell culture in osteogenic inductive extraction. (B) Alizarin Red-S staining after 21 and 28d of cell culture in osteogenic inductive extraction. (C), (D) The quantitative analysis of ALP activity and alizarin Red-S staining. The ALP activity was normalized to the corresponding total protein content. * $p < 0.05$ compared with HA scaffolds. ** $p < 0.01$ compared with HA scaffolds. # $p < 0.05$ compared with HA/Mg scaffolds. ## $p < 0.01$ compared with HA/Mg scaffolds.

3.5 Bioactivity of vascularization *in vitro*

Vascularization is known to provide necessary oxygen and nourishment for reparative cell, tissue ingrowth and bone reconstruction.⁴⁰ It was reported that vascularization could be dependent on the interaction between proteins and divalent

ions (such as Ca^{2+} and Mg^{2+}) since the divalent ions may increase the affinity of some protein receptors in the vascularization process.⁴¹ In this study, the capillary connections formation capability of HUVECs cultured with different vascularized inductive extraction was investigated by microscopy and quantified in terms of the number of capillary connections. Compared with other two groups, HUVECs cultured with extraction of HA/Ca/Mg scaffold after 4h on Matrigel demonstrated a better capillary-like network formation ability (Fig. 7E). The number of capillary connections per field in HA/Ca/Mg scaffold were significantly greater per field than other groups (Fig. 7F, $p < 0.05$). However, the ELISA results (Fig. 7G, $p > 0.05$) illustrated that the released divalent ions did not affect the amount of VEGF secreted by HUVECs, which is an important angiogenic growth factor in the vascularization process.^{42, 43} We hypothesized that divalent ions only increased the sensitivity of HUVECs to VEGF, but did not promote the secretion of VEGF during the vascularization process.

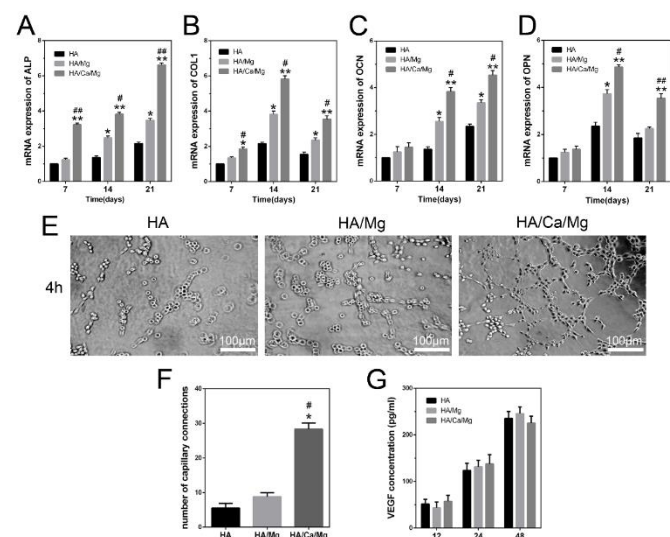


Fig 7. Expression of osteogenic related genes of MC3T3-E1 cells and vascularization evaluation of HUVECs. (A), (B), (C), (D) Relative mRNA expression of osteogenic differentiation related genes in cells grown with various osteogenic inductive extraction measured by real-time PCR after 7, 14 and 21d. (E) Microscopy images of capillary connections formation on Matrigel for 4h by HUVECs after cultured with different vascularized inductive extraction. (F) Total number of capillary connections formation per field by using Image-Pro Plus software. (G) The concentration of VEGF secreted by HUVECs cultured in vascularized inductive extraction for 12, 24 and 48h. * $p < 0.05$ compared with HA scaffolds. ** $p < 0.01$ compared with HA scaffolds. # $p < 0.05$ compared with HA/Mg scaffolds. ## $p < 0.01$ compared with HA/Mg scaffolds.

3.6 Tissue integration and Micro-CT based analysis of vascularization *in vivo*

In tissue regeneration, vascularization can precede osteogenesis, and the enhanced neovascularization can accelerate new bone formation.^{44, 45} It has been demonstrated that angiogenesis is affected by the size of interconnected pore structure, which may lead to a faster vascularization and higher local oxygenation level.²⁶ Three-dimensional images of vascularization within the subcutaneously implanted scaffolds *in vivo* were showed in Fig. 8A, which indicated that more newly formed vessels detected within the HA/Ca/Mg scaffold

compared with HA and HA/Mg scaffolds at 28d after implantation. Meanwhile, the calculated volume of the newly formed vessels within the HA/Ca/Mg scaffold were significantly larger than the other two scaffolds (Fig. 8B, $p < 0.05$). Moreover, histological sections were stained with H&E and Masson's trichrome to assess the soft tissue integration *in vivo*. As demonstrated in Fig. 8C, the HA/Ca/Mg scaffold exhibited better tissue integration than HA and HA/Mg scaffolds, which indicated that the HA/Ca/Mg scaffold could offer a favourable micro-environment for tissue growth. Further, the results of CD31 immunohistochemistry showed a much better neovascularization of the HA/Ca/Mg scaffold than other scaffolds (Fig. 8C). These results showed that the HA/Ca/Mg scaffold displayed better biocompatibility *in vivo* after 28 days from implantation.

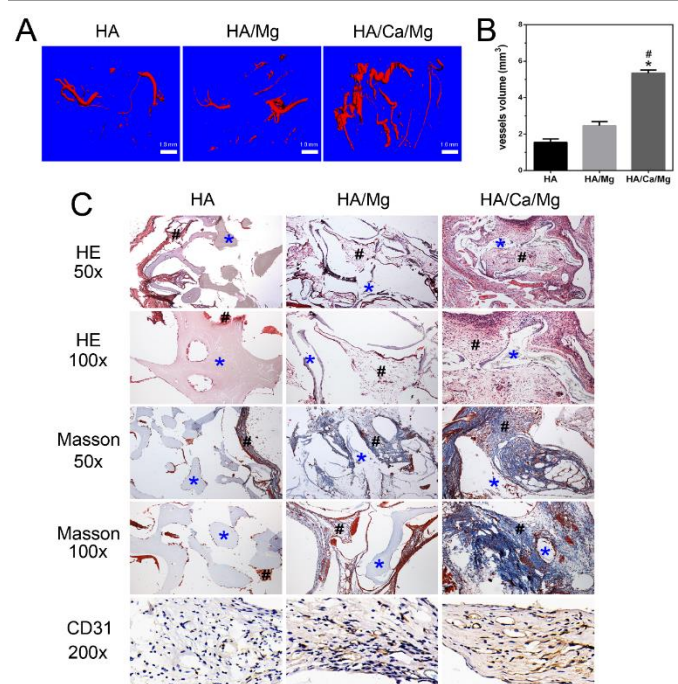


Fig 8. Vascularization and tissue integration of various scaffolds *in vivo*. (A), (B) Representative 3D images of Micro-CT based newly formed vessels within scaffolds at 28d after implantation and quantitative analysis of vessels volume. (C) Histological images of implanted scaffolds at 28d after implantation. H&E and Masson's trichrome staining were used to assess the morphology and tissue integration. CD31 immunohistochemistry was used to assess vascularization (blue *, scaffold; black #, tissue). * $p < 0.05$ compared with HA scaffolds. # $p < 0.05$ compared with HA/Mg scaffolds.

4. Conclusion

We used the hydrothermal calcination process to develop a bioactive scaffold with the original interconnected porous structure and novel nano-crystal whisker-like microstructures on the surface. Moreover, the scaffold can achieve gradient degradation with the capacity of releasing bioactive ions. Our results suggested that this scaffold with the nano-crystal surface effectively enhanced osteogenic cell attachment, spreading, proliferation and focal adhesions formation. Notably, the scaffold promoted the osteogenic differentiation of pre-osteoblasts and capillary connections formation of HUVECs *in vitro* and demonstrated vascularization and tissue

integration *in vivo*. We believe that these factors collectively play a synergistic effect on the biological processes. The unique scaffold developed herein might provide a new class of bioactive degradable composites as bone substitutes or tissue engineering scaffolds capable of osteogenesis and vascularization.

Acknowledgements

This research was financially supported by the National Key R&D Program (2016YFC1102100), Ningbo Municipal Natural Science Foundation (2010C500009) and Zhejiang Natural Science Foundation (2017LY17H060001). X.-P. He thanks the Natural Science Foundation of China (21722801 and 21572058) and the Shanghai Rising-Star Program (16QA1401400) (to X.-P. He) for generous financial support. The Catalysis And Sensing for our Environment (CASE) network is thanked for research exchange opportunities. T. D. J. wishes to thank the Royal Society for a Wolfson Research Merit Award and ECUST for a guest professorship.

Conflict of interest

There are no conflicts of interest to declare.

References

- H. Lu, T. Hoshiba, N. Kawazoe and G. Chen, *Biomaterials.*, 2011, **32**, 2489-2499.
- I. Zderic, P. Steinmetz, L. M. Benneker, C. Sprecher, O. Röhrle, M. Windolf, A. Boger and B. Gueorguiev, *J. Orthop. Transl.*, 2017, **8**, 40-48.
- S. Bhumiratana, W. L. Grayson, A. Castaneda, D. N. Rockwood, E. S. Gil, D. L. Kaplan and G. Vunjak-Novakovic, *Biomaterials.*, 2011, **32**, 2812-2820.
- X. Liu, C. Bao, H. H. Xu, J. Pan, J. Hu, P. Wang and E. Luo, *Acta. Biomater.*, 2016, **42**, 378-388.
- A. Samadikuchaksaraei, M. Gholipourmalekabadi, E. Erfani Ezadyar, M. Azami, M. Mozafari, B. Johari, S. Kargozar, S. B. Jameie, A. Korourian and A. M. Seifalian, *J. Biomed. Mater. Res. A.*, 2016, **104**, 2001-2010.
- M. P. Lutolf, P. M. Gilbert and H. M. Blau, *Nature.*, 2009, **462**, 433-441.
- X. Zhang, H. A. Awad, R. J. O'Keefe, R. E. Guldberg and E. M. Schwarz, *Clin. Orthop. Relat. Res.*, 2008, **466**, 1777-1787.
- I. Bajpai, D. Y. Kim, J. Kyong-Jin, I. H. Song and S. Kim, *J. Biomed. Mater. Res. B Appl. Biomater.*, 2017, **105**, 72-80.
- J.-S. Wang, M. Tägil, H. Isaksson, M. Boström and L. Lidgren, *J. Orthop. Transl.*, 2016, **6**, 10-17.
- Y. Cai, J. Guo, C. Chen, C. Yao, S. M. Chung, J. Yao, I. S. Lee and X. Kong, *Mater. Sci. Eng. C Mater. Biol. Appl.*, 2017, **70**, 148-154.
- C. Chai and K. W. Leong, *Mol. Ther.*, 2007, **15**, 467-480.
- J. Brandt, S. Henning, G. Michler, W. Hein, A. Bernstein and M. Schulz, *J. Mater. Sci. Mater. Med.*, 2010, **21**, 283-294.
- L. Zheng, F. Yang, H. Shen, X. Hu, C. Mochizuki, M. Sato, S. Wang and Y. Zhang, *Biomaterials.*, 2011, **32**, 7053-7059.
- S. V. Dorozhkin, *Acta. Biomater.*, 2010, **6**, 4457-4475.
- X. Li, Y. Zhao, Y. Bing, Y. Li, N. Gan, Z. Guo, Z. Peng and Y. Zhu, *ACS. Appl. Mater. Interfaces.*, 2013, **5**, 5557-5562.
- E. Culverwell, S. C. Wimbush and S. R. Hall, *Chem. Commun. (Camb.)*, 2008, 1055-1057.
- D. Zhao, F. Witte, F. Lu, J. Wang, J. Li and L. Qin, *Biomaterials.*, 2017, **112**, 287-302.
- D. Zhao, S. Huang, F. Lu, B. Wang, L. Yang, L. Qin, K. Yang, Y. Li, W. Li, W. Wang, S. Tian, X. Zhang, W. Gao, Z. Wang, Y. Zhang, X. Xie, J. Wang and J. Li, *Biomaterials.*, 2016, **81**, 84-92.
- X. Chen, *J. Orthop. Transl.*, 2017, **10**, 1-4.
- J. Wei, J. Jia, F. Wu, S. Wei, H. Zhou, H. Zhang, J. W. Shin and C. Liu, *Biomaterials.*, 2010, **31**, 1260-1269.
- R. Ma, S. Tang, H. Tan, J. Qian, W. Lin, Y. Wang, C. Liu, J. Wei and T. Tang, *ACS. Appl. Mater. Interfaces.*, 2014, **6**, 12214-12225.
- C. Li, C. Jiang, Y. Deng, T. Li, N. Li, M. Peng and J. Wang, *Sci. Rep.*, 2017, **7**, 41331.
- H. Tan, S. Guo, S. Yang, X. Xu and T. Tang, *Acta. Biomater.*, 2012, **8**, 2166-2174.
- Y. Yang, S. Yang, Y. Wang, Z. Yu, H. Ao, H. Zhang, L. Qin, O. Guillaume, D. Eglon, R. G. Richards and T. Tang, *Acta. Biomater.*, 2016, **46**, 112-128.
- T. M. Valverde, E. G. Castro, M. H. Cardoso, P. A. Martins-Junior, L. M. Souza, P. P. Silva, L. O. Ladeira and G. T. Kitten, *Life. Sci.*, 2016, **162**, 115-124.
- H. Kokemueller, S. Spalthoff, M. Nolff, F. Tavassol, H. Essig, C. Stuehmer, K. H. Bormann, M. Rucker and N. C. Gellrich, *Int. J. Oral. Maxillofac. Surg.*, 2010, **39**, 379-387.
- H. M. Wong, Y. Zhao, F. K. L. Leung, T. Xi, Z. Zhang, Y. Zheng, S. Wu, K. D. K. Luk, K. M. C. Cheung, P. K. Chu and K. W. K. Yeung, *Adv. Healthc. Mater.*, 2017, **6**.
- H. Zhao, W. Dong, Y. Zheng, A. Liu, J. Yao, C. Li, W. Tang, B. Chen, G. Wang and Z. Shi, *Biomaterials.*, 2011, **32**, 5837-5846.
- S. M. Best, A. E. Porter, E. S. Thian and J. Huang, *J. Eur. Ceram. Soc.*, 2008, **28**, 1319-1327.
- Y. Zhang, J. Xu, Y. Ruan, M. Yu, M. O'Laughlin, H. Wise, D. Chen, L. Tian, D. Shi, J. Wang, S. Chen, J. Feng, D. Chow, X. Xie, L. Zheng, L. Huang, S. Huang, K. Leung, N. Lu, L. Zhao, H. Li, D. Zhao, X. Guo, K. Chan, F. Witte, H. Chan, Y. Zheng and L. Qin, *Nat. Med.*, 2016, **22**, 1160-1169.
- H. S. Roh, C. M. Lee, Y. H. Hwang, M. S. Kook, S. W. Yang, D. Lee and B. H. Kim, *Mater. Sci. Eng. C Mater. Biol. Appl.*, 2017, **74**, 525-535.
- N. Davidenko, C. F. Schuster, D. V. Bax, R. W. Farndale, S. Hamaia, S. M. Best and R. E. Cameron, *J. Mater. Sci. Mater. Med.*, 2016, **27**, 148.
- R. O. Hynes, *Cell*, 1992, **69**, 11-25.
- T. Ohmori, Y. Kashiwakura, A. Ishiwata, S. Madoiwa, J. Mimuro, Y. Furukawa and Y. Sakata, *J. Biol. Chem.*, 2010, **285**, 31763-31773.
- H. Pan, Y. Xie, K. Li, D. Hu, J. Zhao, X. Zheng, T. Tang, *RSC. Adv.*, 2015, **5**, 101834-101842.
- H. Pan, Y. Xie, Z. Zhang, K. Li, D. Hu, X. Zheng, Q. Fan, T. Tang, *Colloid. Surface. B.*, 2017, **152**, 344-353.
- J. Zhang, X. Ma, D. Lin, H. Shi, Y. Yuan, W. Tang, H. Zhou, H. Guo, J. Qian and C. Liu, *Biomaterials.*, 2015, **53**, 251-264.
- B. Leitinger, A. McDowall, P. Stanley and N. Hogg, *Biochim. Biophys. Acta.*, 2000, **1498**, 91-98.
- Y. Shih, Y. Hwang, A. Phadke, H. Kang, N. Hwang, E. Caro, S. Nguyen, M. Siu, E. Theodorakis, N. Gianneschi, K. Vecchio, S. Chien, O. Lee and S. Varghese, *PNAS*, 2014, **111**, 990-995.
- S. Ali, A. Singh, A. A. Mahdi and R. N. Srivastava, *J. Orthop. Transl.*, 2017, **10**, 5-11.
- J. J. Grzesiak, G. E. Davis, D. Kirchhofer and M. D. Pierschbacher, *J Cell Biol*, 1992, **117**, 1109-1117.
- J. He, M. L. Decaris and J. K. Leach, *Tissue. Eng. Part. A.*, 2012, **18**, 1520-1528.
- J. A. Maier, D. Bernardini, Y. Rayssiguier and A. Mazur, *Biochim. Biophys. Acta.*, 2004, **1689**, 6-12.
- S. H. Chen, M. Lei, X. H. Xie, L. Z. Zheng, D. Yao, X. L. Wang, W. Li, Z. Zhao, A. Kong, D. M. Xiao, D. P. Wang, X. H. Pan, Y. X. Wang and L. Qin, *Acta. Biomater.*, 2013, **9**, 6711-6722.

- 45 W. Katagiri, T. Kawai, M. Osugi, Y. Sugimura-Wakayama, K. Sakaguchi, T. Kojima and T. Kobayashi, *Maxillofac. Plast. Reconstr. Surg.*, 2017, **39**, 8.